



Article

Research on Temporal and Spatial Resolution and the Driving Forces of Ecological Environment Quality in Coal Mining Areas Considering Topographic Correction

Xinran Nie ¹, Zhenqi Hu ^{2,*}, Qi Zhu ¹ and Mengying Ruan ¹

¹ Institute of Land Reclamation and Ecological Restoration, China University of Mining and Technology, Beijing 100083, China; xrnie5190@student.cumtb.edu.cn (X.N.); bqt1700204045@student.cumtb.edu.cn (Q.Z.); mengyingruan@student.cumtb.edu.cn (M.R.)

² School of Environment Science and Spatial Informatics, China University of Mining and Technology, Xuzhou 221116, China

* Correspondence: huzq@cumtb.edu.cn; Tel.: +86-1391-063-7448

Abstract: Over the last few years, under the combined effects of climate change and human factors, the ecological environment of coal mining areas has undergone tremendous changes. Therefore, the rapid and accurate quantitative assessments of the temporal and spatial evolution of the ecological environment quality is of great significance for the ecological restoration and development planning of coal mining areas. This study applied the ecological environment index after topographic correction to improve the remote sensing ecological index (RSEI). Based on a series of Landsat images, the ecological environment quality of Yangquan Coal Mine in Shanxi Province from 1987 to 2020 was monitored and evaluated by an improved remote sensing ecological index. The results show that after topographic correction, the topographic effect of the remote sensing ecological index was greatly reduced, and its practicability was improved. From 1987 to 2020, the ecological environment quality of Yangquan Coal Mine was improved, and the mean of the RSEI increased from 0.4294 to 0.6379. The ecological environment quality of the six coal mines in the study area was improved. Among the six coal gangue dumps, the ecological environmental quality of D1, D2, D3, and D4 has improved, and the ecological environment quality of D5 and D6 worsened. The percentages of improved, unchanged, and degraded ecological environment quality in the entire coal mining area were 77.08%, 0.99%, and 21.93%, respectively. The global Moran's index was between 0.7929 and 0.9057, and it was shown that there was a strong positive correlation between the ecological environmental qualities of the study area, and that its spatial distribution was clustered rather than random. The LISA cluster map showed that the aggregation and dispersion degree of ecological environment quality was mainly high–high clustering and low–low clustering over the whole stage. During the study period, temperature and precipitation had limited impacts on the ecological environment quality of Yangquan Coal Mine, while the coal mining activities and urbanization construction seriously affected the local ecological environment quality and the implementation of ecological restoration policies, regulations, and measures was the main reason for the improvement of the ecological environment quality.

Keywords: topographic correction; ecological environment quality; temporal and spatial evolution; driving force; coal mining area



Citation: Nie, X.; Hu, Z.; Zhu, Q.; Ruan, M. Research on Temporal and Spatial Resolution and the Driving Forces of Ecological Environment Quality in Coal Mining Areas Considering Topographic Correction. *Remote Sens.* **2021**, *13*, 2815. <https://doi.org/10.3390/rs13142815>

Academic Editors: Maria Lanfredi, Rosa Coluzzi, Vito Imbrenda and Tiziana Simoniello

Received: 2 June 2021

Accepted: 14 July 2021

Published: 17 July 2021

Publisher's Note: MDPI stays neutral with regard to jurisdictional claims in published maps and institutional affiliations.



Copyright: © 2021 by the authors. Licensee MDPI, Basel, Switzerland. This article is an open access article distributed under the terms and conditions of the Creative Commons Attribution (CC BY) license (<https://creativecommons.org/licenses/by/4.0/>).

1. Introduction

Coal is the most important mineral resource in China and has made great contributions to China's economic development and social progress. In 2020, China's raw coal production was 3.9 billion tons and coal consumption accounted for 56.8% of its total primary energy consumption. For a long period of time in the future, coal will continue to be China's leading energy source [1]. However, the continuous exploitation and utilization of coal

resources are often accompanied by a series of serious ecological and environmental problems, such as vegetation degradation [2], surface subsidence [3], soil erosion [4], air pollution [5], and water resource damage [6]. At present, the surface subsidence area caused by coal mining in China is up to $1.35 \times 10^4 \text{ km}^2$ and increases at a rate of 700 km^2 per year, while the ecological restoration rate of coal mining subsidence is only about 35% [7]. In addition, as the solid waste attached to coal production, more than 6 billion tons of coal gangue have accumulated, and this is increasing at a rate of 795 million tons per year, but the comprehensive utilization rate is lower than 30% [8]. The accumulation of coal gangue not only occupies a large amount of land but is also prone to raising dust and spontaneous combustion, and even causes geological disasters, therefore endangering the ecological safety of the mining area and human health [9]. Particularly in the Loess Plateau, where coal reserves are abundant but the ecological environment is fragile, the above ecological environmental problems are more prominent [10,11]. Therefore, the effective monitoring and evaluation of the surface ecological environment in the coal mining areas of the Loess Plateau is of great significance for the rational development of coal resources and the implementation of ecological restoration strategies by the national and local governments.

Remote sensing technology, with its advantages of a wide monitoring range, fast imaging speed, short revisit period, and low data cost, has been widely applied in the field of ecological environments [12,13], providing an effective means for the quantification and visualization of ecological environment monitoring and evaluation in coal mining areas. For example, the most commonly used normalized difference vegetation index (NDVI) [14] is used to identify the mining disturbance trajectories and to study the vegetation restoration status in coal mining areas [15,16]. The soil adjusted vegetation index (SAVI), modified soil adjusted vegetation index (MSAVI_2), and vegetation coverage (VFC) are used to characterize the impact of coal mining and ecological restoration on the ecological environment of coal mining areas [17,18]. Land surface temperature (LST) can be used to monitor coal field fires and identify surface thermal abnormalities in coal mining areas [19,20]. The modified normalized difference water index (MNDWI) is used to study the dynamic evolution of wetland in coal mining subsidence areas [21]. The soil moisture monitoring index (SSMMI) can effectively assess the soil moisture in coal mining areas [22].

However, the factors affecting the quality of the ecological environment are complex and diverse. The supervision and evaluation of a single indicator can usually only explain the characteristics of the ecological environment in one aspect, and the ecological environment quality of the entire region cannot be reflected in a true and comprehensive manner. It is therefore necessary to integrate a variety of ecological environmental indicators to monitor and evaluate the ecological environmental quality of coal mining areas. Xu et al. [23] applied land use, ecosystem service value, and the ecological storage index to assess the changes in the ecological conditions of coal mining subsidence areas before and after ecological restoration. Xiao et al. [24] selected the 12 indicators of land use, water distribution, terrain relief, proportion of construction, vegetation coverage, desertification rate, rainfall, population density, mining depth, mining thickness, ratio of buried depth versus mining thickness, and mining strength. Based on the index of entropy and linear weighted analysis, an overground-underground model was constructed to quantitatively evaluate the impact of coal mining on the ecosystem of arid mining areas and its resilience. Hou et al. [25] integrated four indicators of geological disasters, soil erosion, vegetation degradation, and environmental pollution, and then used the analytic hierarchy process (AHP) to determine the weight of each indicator, and constructed a comprehensive evaluation model for the ecological environment damage in the Datong coal mining area. Mohammad et al. [26] comprehensively used three indicators of land use/land cover (LULC), vegetation coverage (VFC), and land surface temperature (LST) to assess and predict the impact of mining activities on the ecological environment. However, these comprehensive evaluation methods also have shortcomings; for example, the difficulty of obtaining evaluation indicators, the selection of indicators and the assignment of weights are easily affected by subjective factors, which reduces the accuracy of the evaluation results. Therefore, Xu et al. [27]

proposed a remote sensing ecological index (RSEI) completely based on remote sensing data without a human weight setting. The index uses principal component analysis (PCA) to integrate the four indicators of greenness, wetness, dryness, and heat, and eliminates the limitations of a single indicator. It has been widely used in regional ecological environment quality assessment [28–31].

During the imaging process of remote sensing satellites, the undulating terrain changes the geometric structure of the sun–target–sensor [32], which will cause the solar radiation to be unevenly distributed [33], thereby affecting the accuracy of the radiance and reflectance [34]. Therefore, topographic correction is essential in order to improve the quality of remote sensing images and carry out quantitative research. In the past 40 years, many topographic correction methods have been proposed, which can be roughly divided into three categories: physical models, empirical models, and semi-empirical models. The physical model introduces a physical mechanism to simulate the physical process of the interaction between solar radiation and the Earth's surface. Examples of this are the Cosine-T model [35], Cosine-C model [36], sun canopy sensor (SCS) model [37], and path length correction (PLC) model [38]. The empirical model is based on the statistical relationship between the radiance or reflectance and the cosine (cosi) of the effective angle of incidence. Examples include the statistical empirical (SE) model [35] and the variable empirical coefficient algorithm (VECA) [39]. The semi-empirical model introduces empirical parameters into the physical model, which not only considers the physical mechanism but also uses empirical methods. Examples include the C model [35] and the sun canopy sensor + C (SCS + C) model [40]. Existing evidence shows that topographic correction can not only improve the accuracy of land cover classification [41,42], but also improve the estimation accuracy of net primary productivity (NPP) [43], biomass [44], and leaf area index (LAI) [45].

At present, in the research of ecological environment quality assessment, the influence of topographic factors and the application of a topographic correction model have not been considered. Particularly in the coal mining areas of the Loess Plateau with great topographic fluctuations, the impact of topographic correction on the ecological environment quality assessment of the coal mine area is still unclear. Therefore, this study aims to (1) evaluate the impact of topographic correction on ecological environment quality assessment; (2) analyze the spatial–temporal variation in the ecological environment quality of Yangquan Coal Mine in Shanxi Province from 1987 to 2020 using the remote sensing ecological index (RSEI); (3) reveal the main driving forces of the evolution of ecological environmental quality in coal mining areas.

2. Study Area

Yangquan Coal Mine is located in Yangquan City, Shanxi Province ($37^{\circ}39'–38^{\circ}09'$ N and $113^{\circ}14'–113^{\circ}49'$ E) on the eastern edge of China's Loess Plateau (Figure 1), which is the largest anthracite production base in China. The terrain in the north and west is high, dominated by mountains, while the terrain in the east and south is low, dominated by hills and plains. The overall fluctuation of the terrain is relatively large, and the elevation range is between 474 and 1523 m. The climate is a semi-humid continental monsoon climate in a warm temperate zone. The annual average temperature is $8–12^{\circ}\text{C}$, the number of hours of sunshine is 2700–2900 h, and the annual precipitation is 450–550 mm.

The Yangquan Coal Mine spans the Yangquan municipal district, Yu County, and Pingding County, with a total area of 1737.45 km^2 and 10.2 billion tons of coal reserves. Among the six subordinate coal mines, No. 1 Coal Mine (M1) was established in July 1953 and was put into operation in July 1956. The mine field area is about 83.48 km^2 . No. 2 Coal Mine (M2) was established on 1 May 1951, with a mine field area of approximately 61.62 km^2 . No. 3 Coal Mine (M3) was established in May 1950, with a mine field area of about 39.96 km^2 . No. 4 Coal Mine (M4) was established in January 1950, with a mine field area of approximately 15.90 km^2 . No. 5 Coal Mine (M5) was established in December 1984, with a mine field area of approximately 82.42 km^2 . Xinjing Coal Mine (M6) started

construction in 1990 and was formally established on 1 October 1998. The mine field area is approximately 45.53 km².

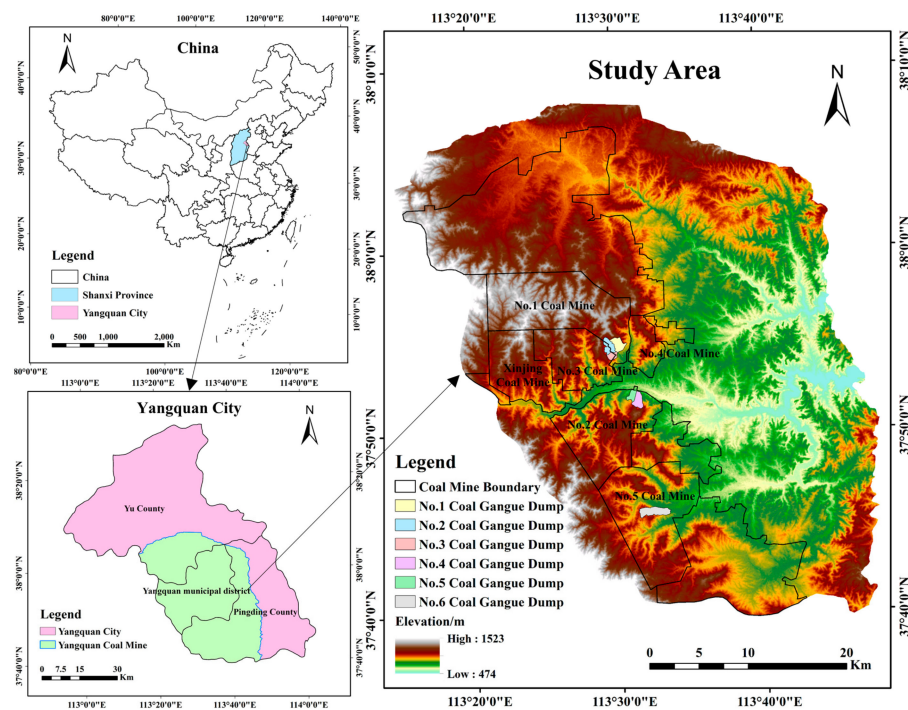


Figure 1. Geographical location of the study area.

There are 148 coal gangue dumps in Yangquan. As shown in Figure 2, this paper focuses on No. 1 coal gangue dump (D1), No. 2 coal gangue dump (D2), No. 3 coal gangue dump (D3), No. 4 coal gangue dump (D4), No. 5 coal gangue dump (D5), and No. 6 coal gangue dump (D6). These dumps are used to analyze the impact of coal gangue spontaneous combustion and ecological restoration on the quality of the ecological environment. D1 was put into use in July 1953 and has been closed for ecological restoration. D2 was put into use in early 2010 and is now operating alongside ecological restoration. D3 was put into use in 2005, and the coal gangue discharge work was completed by the end of 2016. D4 began to accumulate in 1976 and was closed in 2007, with a capacity of about 3.22 million tons. D5 began to accumulate coal gangue in the 1980s and was fully put into use in 2007; by 2020, about 26 million tons of coal gangue had been discharged, and the remaining gangue capacity was about 9 million tons. D6 began to discharge coal gangue in 1992, and is now operating alongside ecological restoration.

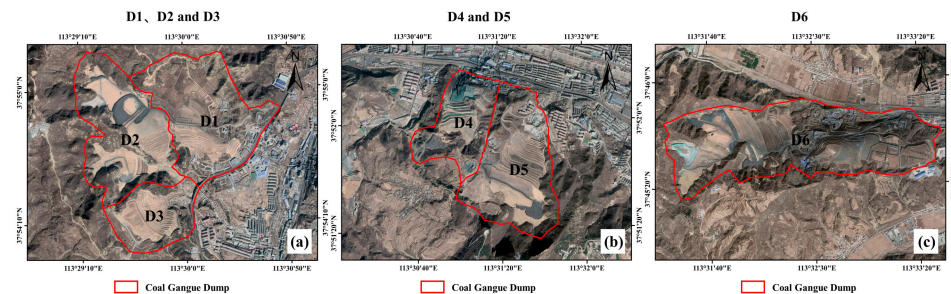


Figure 2. The location of the six coal gangue dumps. (a) The location of the coal gangue dumps D1, D2, and D3; (b) the location of coal gangue dumps D4 and D5; (c) the location of coal gangue dump D6.

3. Materials and Methods

3.1. Data Source and Processing

Landsat data are suitable for long-term and large-scale ecological environmental monitoring. In this study, 48 Landsat-5 TM, Landsat-7 ETM+, and Landsat-8 OLI/TIRS Level 1T images were downloaded. The image spatial resolution was 30 m × 30 m and they were corrected by system radiation correction and geometric correction. All Landsat images were downloaded from the United States Geological Survey (<https://earthexplorer.usgs.gov/> accessed on 13 May 2021). In order to ensure the similarity of vegetation information, all images were selected in August and September. The row/column numbers were 124/34 and 125/34. The solar azimuth angle and elevation angle of each image are shown in Table S1.

Before remote sensing images are used for quantitative research, they must go through a series of preprocessing steps. ENVI 5.3 software was used to preprocess the images, including strip repair, image registration, radiometric calibration, atmospheric correction, cloud detection, image mosaic, and cropping. Firstly, some Landsat ETM+ images were strip repaired using the gap-filling interpolation algorithm of the ENVI 5.3 software. Secondly, all images were rectified to the World Geodetic System (WGS-84) datum and Universal Transverse Mercator (UTM) zone 49N coordinate system, the TM/ETM+ images were co-registered to the OLI/TIRS using second-order polynomial and cubic convolution interpolation re-sampling, and the root mean square error (RMSE) of the registration was found to be less than 0.3 pixels. Thirdly, the “Radiometric Calibration” module of the ENVI 5.3 software was used to calibrate the remote sensing image, and the Fast Line-of-sight Atmospheric Analysis of Spectral Hypercubes (FLAASH) atmospheric correction tool was further used to convert the original digital (DN) value of the Landsat image to ground reflectivity. Clouds and cloud shadows were removed by the Fmask 3.2 cloud detection algorithm [46]. Finally, mosaic work was carried out on the images, and the images of the study area were cut out using the boundary files of the study area.

Object-oriented classification was used to obtain the land cover data of Yangquan Coal Mine in 1987, 1998, 2010, and 2020 (Figure S1 and Table S2). Based on Google Earth satellite images, sample points were selected through visual interpretation to evaluate the accuracy of land cover data. The overall accuracy and kappa coefficients of land cover data were not less than 94.02% and 0.88 (Table S3).

The digital elevation model (DEM) was used for the topographic correction of images. The Advanced Spaceborne Thermal Emission and Reflection Radiometer (ASTER) Global Digital Elevation Model (GDEM) version 2 product with a spatial resolution of 30 m was selected as the DEM data source. The data can be downloaded for free from Geospatial Data Cloud (<http://www.gscloud.cn/> accessed on 13 May 2021).

The precipitation and temperature data of Pingding County, Yangquan City, were from the China Meteorological Data Network (<http://data.cma.cn/> accessed on 13 May 2021). The raw coal production data of Shanxi Province and Yangquan City came from the “Shanxi Statistical Yearbook” and the “China Coal Industry Yearbook”.

3.2. Topographic Correction Model

SCS + C is a model based on a tree canopy which not only takes into account the vertical growth characteristics of trees, but also adjusts the influence of topography and illumination by introducing a semi-empirical coefficient. It has a good topography correction effect in mountainous forest areas [40]. In this study, the SCS + C model was selected to carry out topographic correction on the remote sensing images of the Yangquan Coal Mine area. The formula is as follows:

$$L_m = L \left(\frac{\cos\theta \cos\alpha + C}{\cos i + C} \right). \quad (1)$$

Here, L_m is the radiance or reflectance of the image pixel after correction, L is the pixel radiance or reflectance of the uncorrected image, i is the exitance angles on the horizontal surface, θ is the sun zenith angle, α is the slope angle, and C is the semi-empirical coefficient.

The evaluation of topographic correction in this paper involves four methods: (1) visual assessment: visually analyze whether the difference in the value of the ecological environment index between the shaded and sunny slopes of the mountain is reduced [38]. (2) Correlation analysis: using the square of the correlation coefficient (R^2) and slope value (m) of the cosine of the sun's incidence angle ($\cos i$) and the value of the ecological environment index to evaluate the topographic correction effect. When the correlation coefficient and slope value are 0, the topographic correction effect is the best [44]. (3) Statistical analysis: calculate the mean and standard deviation (SD) of each ecological environment index before and after topographic correction. The ideal topographic correction should keep the mean change small and the standard deviation reduced [42]. (4) The effect of topographic correction is evaluated by the percentage of eigenvalues of the first principal component (PC1) of principal component analysis (PCA). PC1 integrates the information of the four indicators of greenness, humidity, dryness, and heat to the greatest extent, which can be used to represent the ecological environment characteristics of the region [27]. The higher the PC1 feature value percentage is, the more concentrated the information of each indicator is, and the more representative the constructed RSEI is.

3.3. Remote Sensing Ecological Index

The remote sensing ecological index (RSEI) is a comprehensive evaluation index based on the pressure–state–response (PSR) framework. It is constructed from four indicators closely related to the ecological environment: greenness, wetness, dryness, and heat. The four indexes can be represented by the normalized differential vegetation index (NDVI) [14], wetness component (Wet) [47], normalized differential build-up and bare soil index (NDBSI) [29], and land surface temperature (LST) [48].

3.3.1. Greenness Index

The normalized difference vegetation index (NDVI) is the most widely applied vegetation index. It is closely related to vegetation parameters such as chlorophyll, vegetation coverage, plant biomass, vegetation productivity, and leaf area index, and is the best indicator of vegetation growth status and health [49]. The NDVI is more sensitive to low-density vegetation, so it is especially suitable for coal mining areas [50]. The formula is as follows:

$$\text{NDVI} = (\rho_{\text{NIR}} - \rho_{\text{Red}}) / (\rho_{\text{NIR}} + \rho_{\text{Red}}). \quad (2)$$

Here, ρ_{NIR} and ρ_{Red} represent the reflectance of the near-infrared band and the red band, respectively.

3.3.2. Humidity Index

The wetness index is expressed by the wetness component (Wet) calculated by the tasseled cap transformation (TCT). The wetness component can intuitively reflect the wetness of surface vegetation and soil [51]. The wetness component formulas of TM, ETM+, and OLI are as follows:

$$\text{Wet}_{\text{TM}} = 0.0315\rho_{\text{Blue}} + 0.2012\rho_{\text{Green}} + 0.3102\rho_{\text{Red}} + 0.1594\rho_{\text{NIR}} - 0.6806\rho_{\text{SWIR1}} - 0.6109\rho_{\text{SWIR1}}. \quad (3)$$

$$\text{Wet}_{\text{ETM+}} = 0.2626\rho_{\text{Blue}} + 0.2141\rho_{\text{Green}} + 0.3102\rho_{\text{Red}} + 0.0656\rho_{\text{NIR}} - 0.7629\rho_{\text{SWIR1}} - 0.5388\rho_{\text{SWIR1}}. \quad (4)$$

$$\text{Wet}_{\text{OLI}} = 0.1511\rho_{\text{Blue}} + 0.1973\rho_{\text{Green}} + 0.3283\rho_{\text{Red}} + 0.3407\rho_{\text{NIR}} - 0.7117\rho_{\text{SWIR1}} - 0.4559\rho_{\text{SWIR2}}. \quad (5)$$

Here, ρ_i is the reflectance of each band of the TM, ETM+, and OLI sensors, respectively.

3.3.3. Dryness Index

Frequent mining activities and rapid urban development have gradually replaced the original surface natural landscape with buildings and bare soil, which has accelerated the

dryness of the land surface and had a negative impact on the ecological environment of the region. Therefore, the index-based built-up index (IBI) [52] and the soil index (SI) [53] can be used to construct a normalized differential build-up and bare soil index (NDBSI) to represent the dryness of the remote sensing ecological index (RSEI). This is calculated as follows:

$$\text{NDBSI} = (\text{IBI} + \text{SI})/2, \quad (6)$$

$$\text{IBI} = \{2\rho_{SWIR1}/(\rho_{SWIR1} + \rho_{NIR}) - [\rho_{NIR}/(\rho_{NIR} + \rho_{Red}) + \rho_{Green}/(\rho_{Green} + \rho_{SWIR1})]\} / \{2\rho_{SWIR1}/(\rho_{SWIR1} + \rho_{NIR}) + [\rho_{NIR}/(\rho_{NIR} + \rho_{Red}) + \rho_{Green}/(\rho_{Green} + \rho_{SWIR1})]\}, \quad (7)$$

$$\text{SI} = [(\rho_{SWIR1} + \rho_{Red}) - (\rho_{NIR} + \rho_{Blue})] / [(\rho_{SWIR1} + \rho_{Red}) + (\rho_{NIR} + \rho_{Blue})]. \quad (8)$$

Here, ρ_i is the reflectance of each band of the TM, ETM+, and OLI sensors, respectively.

3.3.4. Heat Index

The heat index can be expressed by the land surface temperature (LST). In this study, the 6th band of Landsat-5 TM, the 6th band of Landsat-7 ETM+, and the 10th band of Landsat-8 OLI/TIR were used to retrieve the surface temperature. The calculation formulas for LST are as follows:

$$L_\lambda = \text{gain} \times \text{DN} + \text{bias}, \quad (9)$$

$$T_b = K_2 / \ln(K_1 / L_\lambda + 1), \quad (10)$$

$$\text{LST} = T_b / [1 + (\lambda T_b / \rho) \ln \varepsilon] - 273. \quad (11)$$

Here, L_λ is the radiance of the thermal infrared band, which corresponds to the radiance of the 6th band of Landsat-5 TM, the 6th band of Landsat-7 ETM+, and the 10th band of Landsat-8 OLI/TIR; *gain* and *bias* are the gain value and bias value of the corresponding band, which can be obtained from the image header file; T_b is the brightness temperature of the satellite; K_1 and K_2 are thermal calibration parameters. For the 6th band of Landsat-5 TM, $K_1 = 607.76 \text{ W}/(\text{m}^2 \cdot \text{sr} \cdot \mu\text{m})$ and $K_2 = 1260.56 \text{ K}$. For the 6th band of Landsat-7 ETM+, $K_1 = 666.09 \text{ W}/(\text{m}^2 \cdot \text{sr} \cdot \mu\text{m})$ and $K_2 = 1282.71 \text{ K}$. For the 10th band of Landsat-8 OLI/TIR, $K_1 = 774.89 \text{ W}/(\text{m}^2 \cdot \text{sr} \cdot \mu\text{m})$ and $K_2 = 1321.08 \text{ K}$. λ is the center wavelength of the thermal infrared band, $\rho = 1.438 \times 10^{-2} \text{ (mK)}$, and ε is the surface emissivity.

3.3.5. Construction of Remote Sensing Ecological Index

This study uses principal component analysis (PCA) to integrate the NDVI, Wet, NDBSI, and LST to construct the remote sensing ecological index (RSEI). PCA is a multi-dimensional data compression technology which can not only eliminate the influence of collinearity among variables, but also automatically calculate the weight according to the contribution degree of each index to each principal component and concentrate the main information of all indexes on 1–2 principal components [54]. Since the magnitudes and units of the four indicators are inconsistent, the value of each indicator must be standardized between 0 and 1 before the principal component analysis takes place. The standardized formula is as follows:

$$NI_i = (I_i - I_{min}) / (I_{max} - I_{min}). \quad (12)$$

Here, NI_i is the standardized index value, I_i refers to the index value at pixel i , and I_{max} and I_{min} are the maximum and minimum values of the index, respectively.

We calculated the first principal component (PC1) for the four normalized indicators to obtain the initial RSEI value. The initial RSEI calculation formula is as follows:

$$\text{RSEI} = \text{PC1}[f(\text{NDVI}, \text{Wet}, \text{NDBSI}, \text{LST})]. \quad (13)$$

The formula for reverse processing is:

$$\text{RSEI} = 1 - \text{PC1}[f(\text{NDVI}, \text{Wet}, \text{NDBSI}, \text{LST})]. \quad (14)$$

In order to facilitate the study of the change in RSEI, we applied Formula (12) to standardize the initial RSEI value calculated between 0 and 1 to obtain the RSEI value. The closer the RSEI is to 1, the better the ecological environment is, and vice versa. According to previous studies [55,56], the RSEI can be divided into 5 levels: excellent (0.8–1.0), good (0.6–0.8), moderate (0.4–0.6), fair (0.2–0.4), and poor (0–0.2).

3.4. Spatial Auto-Correlation Analysis

Spatial auto-correlation refers to whether the eco-environmental quality of an element is potentially interdependent with the eco-environmental quality of its adjacent space [57]. Moran's index is a commonly used spatial auto-correlation analysis index and includes global Moran's index and local Moran's index. Global Moran's index is used to study the global spatial correlation of the RSEI, and local Moran's index is used to study the local spatial aggregation characteristics of the RSEI. They are calculated as follows:

$$\text{Global Moran's Index} = \frac{n \sum_{i=1}^n \sum_{j=1}^m W_{ij}(x_i - \bar{x})(x_j - \bar{x})}{\left(\sum_{i=1}^n \sum_{j=1}^m W_{ij} \right) \sum_{i=1}^n (x_i - \bar{x})^2}, \quad (15)$$

$$\text{Local Moran's Index} = \frac{n(x_i - \bar{x}) \sum_{j=1}^m W_{ij}(x_j - \bar{x})}{\sum_{i=1}^n (x_i - \bar{x})^2}. \quad (16)$$

Here, n is the number of spatial units in the study area; x_i and x_j are the RSEI values (attribute values) of spatial units i and j , respectively; \bar{x} is the mean value of the RSEI; W_{ij} is the spatial weight matrix. The Moran's index value ranges from -1 to 1 . The closer the absolute value of I is to 1 , the stronger the spatial auto-correlation is. If $I > 0$, it is a positive correlation; if $I < 0$, it is a negative correlation; if $I = 0$, it means that there is no spatial auto-correlation. Local Moran's index is usually visualized by the local indicator of spatial association (LISA). The results of the LISA graph can be divided into five categories: not significant, high-high (HH), low-low (LL), low-high (LH), and high-low (HL). Both global Moran's index and local Moran's index were calculated using Geoda software.

4. Results

4.1. Temporal and Spatial Evolution of Ecological Environment Quality in Coal Mine Area

4.1.1. Temporal Evolution of Ecological Environment Quality

As shown in Figure 3, during the study period, the ecological environment quality of Yangquan Coal Mine showed an overall upward trend. In 1987, the mean of the RSEI was the lowest in history (0.4294), and the proportion of areas with fair and medium ecological environment quality exceeded 60%. By 1998, the mean of the RSEI had increased to 0.5059, and the total area with a good or excellent ecological environment quality was almost equal to the total area with poor and fair ecological environment quality; these were 35.15% and 33.47%, respectively. During this period, the ecological environment quality in the study area steadily improved. From 1998 to 2010, the mean of the RSEI increased by 0.15, the corresponding total area of good and excellent ecological environment quality increased by 36.58%, and the total area of poor and average ecological environment quality decreased by 18.74%, indicating the continuous improvement of ecological environment quality in the study area. From 2010 to 2020, the mean of the RSEI decreased from 0.6559 to 0.6379. Although the proportion of excellent areas increased slightly by 1.31%, the proportion of good areas decreased to 36.06%. In addition, the proportions of poor, average, and moderate areas increased from 7.57%, 7.16%, and 13.54% to 8.66%, 9.26%, and 16.6%, respectively. During this period, the ecological environment quality of the study area showed degradation.

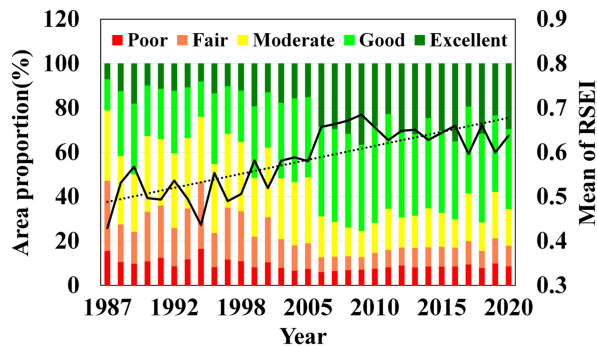


Figure 3. The mean of RSEI and the area proportions of different RSEI grades of Yangquan Coal Mine from 1987 to 2020.

Figure 4 shows the mean of the RSEI and the proportion of the RSEI grades of coal mines and coal gangue dumps in Yangquan from 1987 to 2020. The mean of the RSEI of M1, M2, M3, M5, and M6 all showed upward trends from 1987 to 2010. The proportions of areas of the five coal mines with good and excellent ecological environment quality all increased, while the proportions of areas with poor, fair, and moderate ecological environment quality all decreased. From 2010 to 2020, the mean of the RSEI of the five coal mines showed a fluctuating downward trend and the total areas with good and excellent ecological environment quality decreased, while the total areas with poor, average, and moderate ecological environment quality increased correspondingly. During the study period, the mean of the RSEI of M4 was between 0.48 and 0.62, showing a steady upward trend overall (Figure 4e).

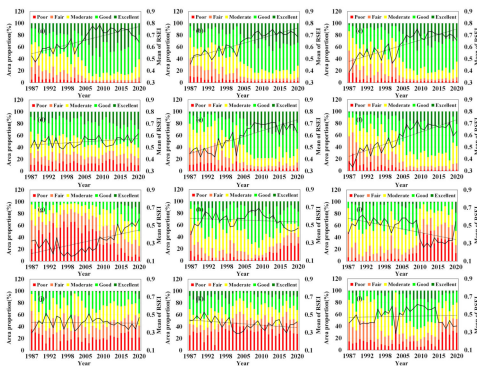


Figure 4. The mean of RSEI and the area proportions of the RSEI grades of the coal mines and coal gangue dumps in Yangquan from 1987 to 2020. (a–f), The mean RSEI and the area proportions of the RSEI grades of M1, M2, M3, M4, M5, and M6 coal mines, respectively. (g–l) The mean RSEI and the area proportions of the RSEI grades of D1, D2, D3, D4, D5, and D6 coal gangue dumps, respectively.

From 1987 to 2020, the ecological environment quality of D1, D2, D3, and D4 improved and the ecological environment quality of D5 and D6 deteriorated. Among them, after large-scale spontaneous combustion occurred in 1993, the mean of the RSEI of D1 was only 0.178. After fire-extinguishing treatment and vegetation restoration, the mean of the RSEI rapidly increased to 0.3653 in 1994, and a large-scale reignition occurred in 1996, resulting in poor and fair ecological environmental quality over a long period of time (Figure 4g). The mean of the RSEI did not decrease immediately after D2 and D3 were put into use and remained stable or even slightly increased within 4–5 years. This is because the ecological environment has the ability of natural restoration, and the undisturbed area in the coal gangue dump relies on natural business forces to continue to develop in the direction of good ecological environment quality. When natural restoration cannot offset the negative impact of coal gangue accumulation and spontaneous combustion

on the ecological environment, the mean of the RSEI will continue to decrease rapidly. Spontaneous combustion occurred many times in the local areas of D4 and D5, which resulted in them having the lowest means of the RSEI (0.2957 and 0.2906) in 1987 and 2002, respectively (Figure 4j,k). From 1987 to 2001, the mean of the RSEI of D6 showed an upward trend (Figure 4l). In 2002, local spontaneous combustion occurred in D6 and the mean of the RSEI dropped rapidly to 0.2829. After ecological restoration, the mean of the RSEI from 2004 to 2014 was maintained above 0.49, and the overall performance of the ecological environment quality was moderate and good. After 2014, the mean of the RSEI continued to decrease, reaching 0.3701 in 2020. The ecological environment quality was mainly poor, fair, or moderate. From a broad point of view, among the six coal gangue dumps, the cumulative annual average of the mean of the RSEI of D2 is the highest (0.556), indicating that D2 has the best ecological restoration effect.

4.1.2. Spatial Evolution of Ecological Environment Quality

Figure 5 shows the spatial distribution of the RSEI grades in the study area. In 1987, the areas with good and excellent ecological environment quality were mainly distributed on the western border and in some parts of the central region where with dense vegetation (Figure S1). The poor and fair areas of ecological environment quality were distributed in the eastern, northern, and western coal mine areas with more construction land and bare soil. By 1998, the vegetation area of the study area had increased by 18.07 km² and the bare soil area had decreased by 22.69 km² (Figure S2). The ecological environment in the central, northern, and western coal mining areas was obviously improved, but the ecological environment quality in the eastern area was still poor and fair. In 2002, areas with poor and fair ecological environments began to shrink back to the central and northern regions. In 2006, spatial patterns of poor and fair ecological environmental quality in the central and northern regions and patterns of good and excellent ecological environmental quality in the eastern and western regions were formed. From 2010 to 2020, with the decrease in vegetation and the increase in construction land in the study area, the regions with good and excellent ecological environment quality showed a slow shrinking trend, while the regions with poor, fair, and moderate ecological environment quality showed a slow expansion trend. As shown in Figures S1–S3, the good and excellent plaques in D1 continued to increase, while the poor and fair plaques in D2, D3, D4, D5, and D6 gradually expanded after they were put into use. After ecological restoration, poor and fair areas were gradually replaced by good and excellent areas.

In order to further study the spatial difference in the ecological environment quality changes in Yangquan Coal Mine, the image difference method was used to detect changes in the RSEI of Yangquan Coal Mine from 1987 to 2020 (Figure 6). The results of the RSEI change detection can be divided into nine levels and three categories. The range of the levels is from −4 to 4. A positive value indicates that the ecological environment is improved, a value of zero indicates that the ecological environment has not changed, and a negative value indicates that the ecological environment is degraded. As shown in Table 1, from 1987 to 1998, the areas with an improved ecological environment accounted for 64.55% of the entire study area and were mainly distributed in the northern area and the western coal mining area. Areas with no changes in the ecological environment accounted for only 1.31%. The areas with a degraded ecological environment accounted for 34.14% and were mainly distributed in the lower elevation area in the east, the Yu County cluster in the north, and the central area. From 1998 to 2010, the ecological environment in the east was greatly improved and the ecological environment in the Yu County cluster in the north and the central region continued to degrade. From 2010 to 2020, the areas with a degraded ecological environment accounted for 52.08% and were distributed in the southeast and west, while areas with an improved ecological environment accounted for less than 50% and were distributed in the northeast and central areas. During this period, the degree of degradation of the ecological environment in the study area exceeded the degree of improvement of the ecological environment.

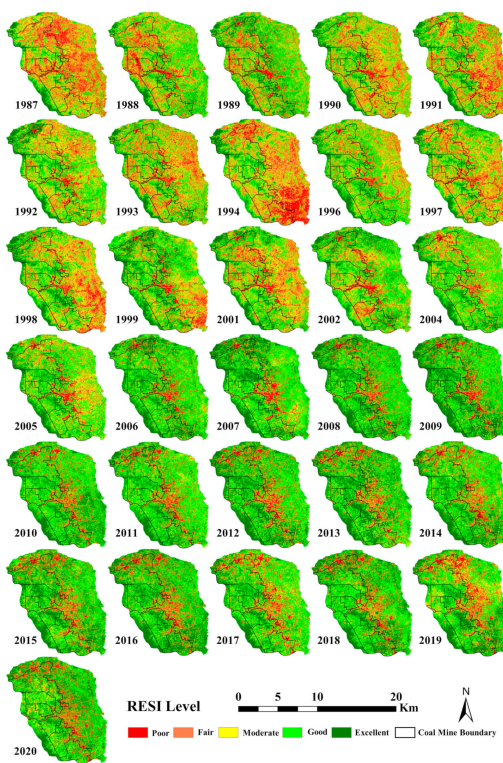


Figure 5. Spatial distribution of RSEI grades in Yangquan Coal Mine from 1987 to 2020.

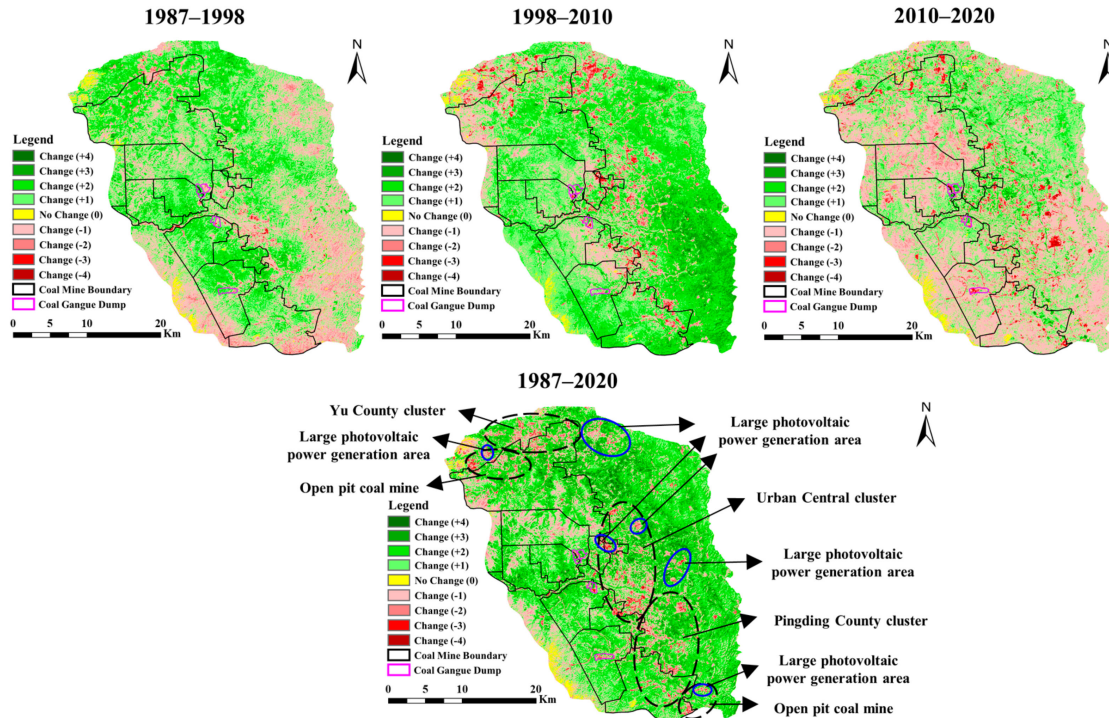


Figure 6. Change detection image of RSEI in Yangquan Coal Mine from 1987 to 2020.

Table 1. Percentage change of the ecological environment quality level in Yangquan Coal Mine from 1987 to 2020.

Type	Level	1987–1998		1998–2010		2010–2020		1987–2020	
		Level Percent (%)	Sub-Total (%)						
Improved	+4	0.06		0.27		0.19		1.67	
	+3	1.49	64.55	6.07	77.07	0.92	46.47	12.96	77.08
	+2	17.65		27.68		5.18		32.26	
	+1	45.35		43.05		40.18		30.19	
Unchanged	0	1.31	1.31	1.15	1.15	1.45	1.45	0.99	0.99
Degraded	-1	29.22		15.83		42.94		15.81	
	-2	4.49	34.14	3.97	21.78	6.48	52.08	4.83	21.93
	-3	0.37		1.70		2.11		1.14	
	-4	0.06		0.28		0.55		0.15	

Throughout the entire study period (1987–2020), the area of ecological environment improvement in the study area was 1339.23 km², accounting for 77.08% of the study area, and the grade changes were mainly concentrated in +1, +2, and +3. The area where there was no change in the ecological environment was 17.2 km², with a percentage of 0.99%, most of which was located in mountainous areas in the northeast and southwest. The area with ecological environment degradation was 281.02 km²; the percentage was 21.93%; and it was mainly distributed in the northern, central, and western coal mining areas. The degraded areas of the ecological environment in the north and the middle include the urban central cluster, Yu County cluster, and Pingding County cluster, indicating that the continuous advancement of urbanization has had a negative impact on the ecological environment. The degraded areas of the ecological environment in the north and the middle include the central district of Yangquan City, Yu County cluster, and Pingding County cluster, indicating that the continuous advancement of urbanization has had a negative impact on the ecological environment. The degradation grades of the western coal mining areas are mostly -1 and -2, while the degradation grades of No. 2, No. 5, and No. 6 coal gangue dumps and coal mining subsidence areas have reached -3 and -4. Table S4 also shows that in the three periods of 1987–1998, 1998–2010, and 2010–2020, the proportion of ecological environment degradation within the boundaries of mineral rights has shown a continuous increasing trend. This shows that coal mining, coal gangue accumulation, and spontaneous combustion restrict the sustainable development of the ecological environment in coal mining areas.

4.1.3. RSEI Modeling and Prediction

In order to quantitatively describe the characteristics of the ecological environment of the coal mining area, 41,502 sample points were collected for each of the NDVI, Wet, NDBSI, LST, and RSEI images each year, with the RSEI as the dependent variable and the NDVI, Wet, NDBSI, and LST as the independent variables for a stepwise regression analysis (Figure S5). The regression models of the study area in 1987, 1998, 2010, and 2020 were as follows (significant at the 0.01 level):

Yangquan Coal Mine in 1987:

$$\text{RSEI} = 0.2794\text{NDVI} + 0.2850\text{Wet} - 0.4128\text{NDBSI} - 0.2918\text{LST} + 0.5563 \quad (R^2 = 0.9957). \quad (17)$$

Yangquan Coal Mine in 1998:

$$\text{RSEI} = 0.2916\text{NDVI} + 0.2422\text{Wet} - 0.4040\text{NDBSI} - 0.3157\text{LST} + 0.5702 \quad (R^2 = 0.9972). \quad (18)$$

Yangquan Coal Mine in 2010:

$$\text{RSEI} = 0.3782\text{NDVI} + 0.2129\text{Wet} - 0.3621\text{NDBSI} - 0.2374\text{LST} + 0.4929 \quad (R^2 = 0.9983). \quad (19)$$

Yangquan Coal Mine in 2020:

$$\text{RSEI} = 0.3511\text{NDVI} + 0.2456\text{Wet} - 0.3842\text{NDBSI} - 0.2077\text{LST} + 0.4809 \quad (R^2 = 0.9987). \quad (20)$$

From Formulas (17)–(20), it can be seen that the four indicators are retained after stepwise regression, indicating that the four indicators are all important factors that regulate the ecological environment in the study area. Using Formulas (21) and (22), the difference and difference percent for each year's indicators were calculated, respectively.

$$\text{Difference} = (|\text{NDBSI}| + |\text{LST}|) - (\text{NDVI} + \text{Wet}) \quad (21)$$

$$\text{Difference percent} = \{[(|\text{NDBSI}| + |\text{LST}|)/(\text{NDVI} + \text{Wet})] - 1\} \times 100\% \quad (22)$$

As shown in Table 2, the coefficients of NDVI and Wet are positive, which means they have a positive effect on the ecological environment, and the coefficients of the NDBSI and LST are negative, which means they have a negative effect on the ecological environment. From the difference and difference percent, it can be seen that in 1987, 1998, and 2010, the comprehensive influence of the NDVI and Wet, which had a positive effect on the ecological environment, was less than that of the NDBSI and LST, which had a negative effect on the ecological environment, as the sum of the coefficients of the NDVI and Wet is less than the sum of the absolute values of the coefficients of the NDBSI and LST. In 2020, this situation was changed. The difference and difference percent are both negative numbers, indicating that the comprehensive influence of the NDVI and Wet, which have a positive effect on the ecological environment, is higher than that of the NDBSI and LST, which have a negative effect on the ecological environment.

Table 2. Coefficient comparison of regression models.

Year	NDVI	Wet	NDBSI	LST	Difference	Difference Percent (%)
1987	0.2794	0.2850	-0.4128	-0.2918	0.1402	24.84
1998	0.2916	0.2422	-0.4040	-0.3157	0.1859	34.83
2010	0.3782	0.2129	-0.3621	-0.2374	0.0084	1.42
2020	0.3511	0.2456	-0.3842	-0.2077	-0.0048	-0.80
Mean	0.3251	0.2464	-0.3908	-0.2632	0.0824	14.42

In summary, the NDVI and NDBSI had the greatest impact on the ecological environment of coal mining areas. Therefore, using the 2020 regression model for predictions, in the future, it is evident that we only need to increase the NDVI by 0.2848 units or reduce the NDBSI by 0.2603 units to increase the RSEI by 0.1 units.

4.2. Spatial Auto-Correlation Analysis of RSEI in Coal Mine Area

As shown in Figure 7, global Moran's index of the RSEI in Yangquan Coal Mine is all positive values, with a cumulative annual average of 0.857, indicating that there is a strong spatial auto-correlation between the RSEI in the study area. Global Moran's index showed an overall fluctuating growth trend, indicating that the spatial distribution of the RSEI is clustered rather than random. As time goes by, the degree of spatial clustering shows a gradual increasing trend.

We used the LISA cluster map to evaluate the local spatial clustering characteristics of the RSEI in the Yangquan Coal Mine. The LISA cluster map of the four years is dominated by high-high clustering and low-low clustering, while the distribution of low-high clustering and high-low clustering is relatively scattered and not obvious (Figure 8). In 1987 and 1998, the high-high clustering was mainly located in the western coal mining area and the western boundary of the study area, while it was more scattered in the eastern area. Low-low clusters were mainly distributed in the central urban area and eastern area of the study area. In 2010, the high-high clusters were distributed in the west and southeast, while the low-low clusters expanded to the middle and north. In 2020, the high-high

clusters were expanded to the northeast and gradually surrounded the low–low clusters in the central and northern regions.

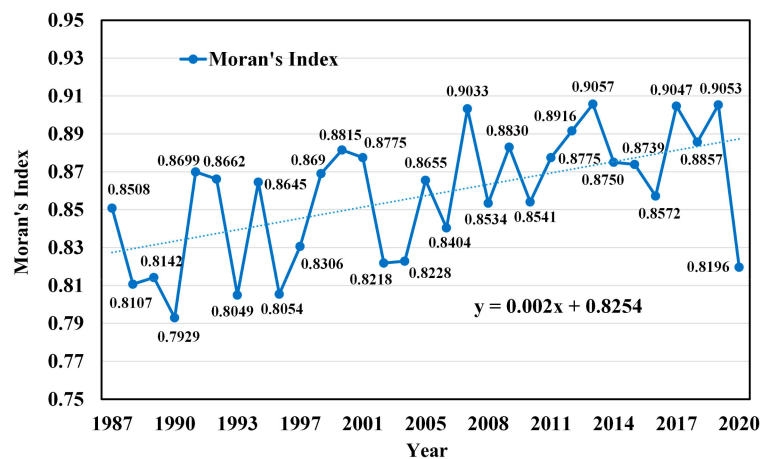


Figure 7. Global Moran's index of the RSEI of Yangquan Coal Mine from 1987 to 2020.

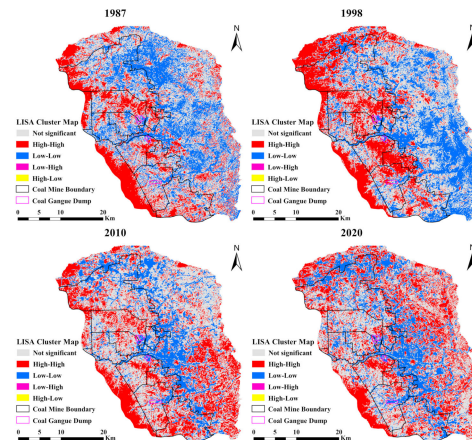


Figure 8. LISA cluster map of RSEI in Yangquan Coal Mine.

4.3. Comparison of Ecological Environment Indicators before and after Topographic Correction

The ecological environment indicators used in this study were corrected by SCS + C. Therefore, it is necessary to compare the differences in ecological environment indicators before and after topographic correction. As shown in Figure 9, after topographic correction, the three-dimensional relief effect of the image was significantly reduced, the index values of the shaded and sunny slopes tended to be the same, and the spatial details were more abundant. Through correlation analysis, statistical analysis, and the percentage of PC1 eigenvalues, the influence of topographic correction on ecological environment indicators was quantitatively studied. The results show that the R^2 and m values of each index value were greatly reduced after topographic correction (Figure S5), indicating that the SCS + C model successfully suppressed the terrain effect of each ecological environment index. Table S5 and Figure S6 show that the average value of each ecological environment index was relatively stable before and after the topographic correction, and that the standard deviation of each index after the topographic correction was reduced to varying degrees. It can be seen from Table S6 that the percentages of the PC1 eigenvalues were improved to varying degrees after topographic correction. This shows that the interpretation ability of PC1 was enhanced after topographic correction, and the constructed RSEI was also more convincing. Therefore, the RSEI with topographic correction was more suitable than the RSEI without topographic correction for evaluating the ecological environment quality in the Yangquan Coal Mine area.

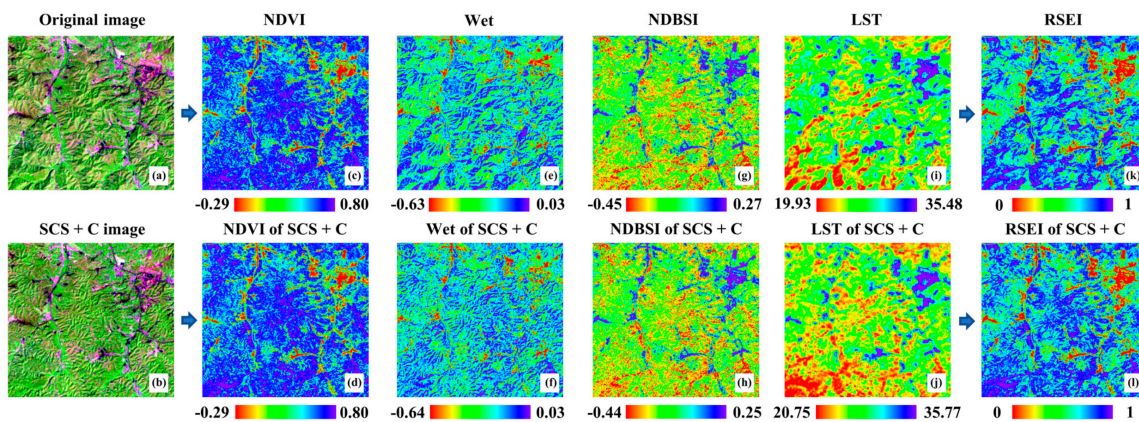


Figure 9. Comparison of the ecological environment indexes before and after topographic correction. (a) Original image, (b) SCS + C image, (c) NDVI image, (d) NDVI image corrected by SCS + C, (e) Wet image, (f) Wet image corrected by SCS + C, (g) NDBSI image, (h) NDBSI image corrected by SCS + C, (i) LST image, (j) LST image corrected by SCS + C, (k) RSEI image, and (l) RSEI image corrected by SCS + C.

5. Discussion

5.1. Analysis of Driving Forces for Changes in Ecological Environment Quality in Coal Mining Areas

As we all know, changes in ecological environment quality are affected by many factors, which can be roughly divided into natural factors and human factors [58]. In the special area of the coal mining area of the Loess Plateau, climate is an important natural factor and its impact on the ecological environment cannot be ignored [24]. Human factors, as the main driving force behind changes in the quality of the ecological environment in coal mining areas, have a more far-reaching impact, including coal mining activities, ecological restoration, and urbanization.

5.1.1. Climate Change

Temperature and precipitation are the two indicators that are most commonly used to describe climate change [59]. According to the data from the Pingding County Meteorological Station in Yangquan City, the average temperature from August to September, the average annual temperature, and the annual precipitation in the study area from 1987 to 2019 showed an overall increasing trend, while the precipitation from August to September showed a decreasing trend (Figure 10). In order to further explore the impact of climate change on the ecological environment, this study uses the Pearson correlation analysis method to analyze the correlation between climate variables and the mean of the RSEI. As shown in Table S7, the correlation coefficients between the annual precipitation, the precipitation from August to September, and the mean of the RSEI of Yangquan Coal Mine are 0.361 and 0.380. The correlation coefficient between the average temperature from August to September and the mean of the RSEI of D6 is -0.364 . The above correlations all passed the 0.05 significance test. The results show that the average temperature from August to September has a certain negative impact on D6 and has little impact on the entire study area. Precipitation is one of the main factors that can change the ecological environment quality of Yangquan Coal Mine, but it has limited impact on the ecological environment of other coal mines and coal gangue dumps. Therefore, we believe that the changes in the ecological environment quality in the study area may also be related to human factors.

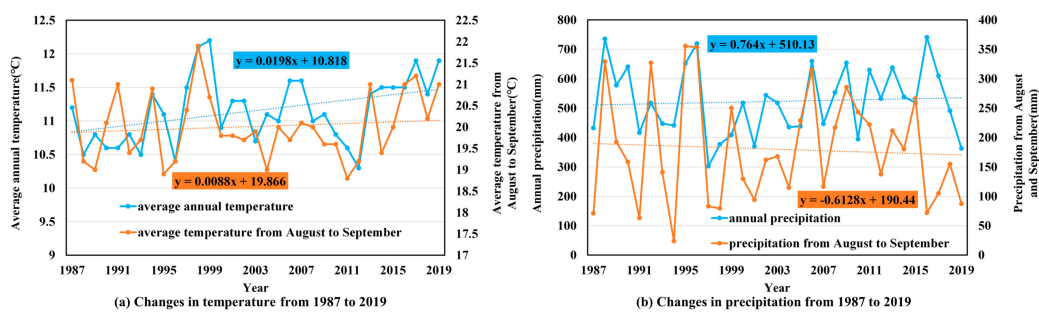


Figure 10. Changes in annual average temperature and annual precipitation in Pingding County, Yangquan City, from 1987 to 2019. (a) Changes in temperature from 1987 to 2019, (b) changes in precipitation from 1987 to 2019.

5.1.2. Coal Mining Activities

Coal mining activities are one of the main driving factors for the temporal and spatial changes in the ecological environment quality in coal mining areas. From 1987 to 2020, the coal mining industry in Shanxi Province and Yangquan City experienced a period of vigorous development, with raw coal production increasing by 328.33% and 459.59%, respectively (Figure 11). Frequent mining activities have greatly promoted the rise and development of coal resource-based cities in Shanxi Province and also had a negative impact on the local ecological environment [11,18,25]. Yangquan Coal Mine is located in the Loess Plateau with a fragile ecological environment. Large-scale mining operations have destroyed the local land use structure and landscape pattern, making the region vulnerable to serious soil erosion [60]. There is evidence that, affected by coal mining and land use changes, the original vegetation of Yangquan Coal Mine has been completely changed or destroyed, which has caused tremendous pressure on the ecological environment of the local and surrounding areas [61]. During the periods of 1987–1998, 1998–2010, and 2010–2020, the area with evident ecological environment degradation within the boundary of mining rights gradually increased (Table S4), reaching 180.63, 183.15, and 415.82 km², respectively. The continuous coal mining activities have a negative impact on the local ecological environment. In addition, in the process of coal mining and processing, a large amount of coal gangue is produced. Due to the spontaneous combustion characteristics of coal gangue, fires often occur in coal gangue storage dumps, which are common in Yangquan Coal Mine [62]. The spontaneous combustion of coal gangue causes the soil temperature to rise, causing damage and even death to the roots of the vegetation. At the same time, under the action of high temperatures, the evaporation rate of soil moisture is accelerated and the dryness of the surface increases [20]. The six coal gangue dumps studied in this paper all experience spontaneous combustion to varying degrees. The areas of spontaneous combustion often correspond to lower RSEI values and poor ecological environment quality levels. In addition, the annual average of the mean of the RSEI of the six coal gangue dumps is lower than the level across the entire study area (0.583). It can be seen that the repeated spontaneous combustion of the coal gangue dump is an important factor restricting the development of the ecological environment of Yangquan Coal Mine.

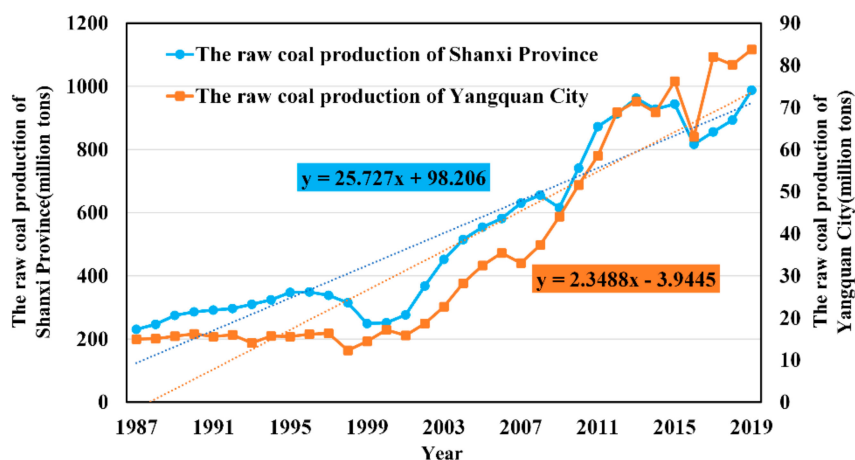


Figure 11. Raw coal production in Shanxi Province and Yangquan City from 1987 to 2019.

5.1.3. Ecological Restoration

Ecological restoration is the main reason for the improvement in the ecological environment of Yangquan Coal Mine. Since the 1980s, the Chinese government and relevant departments have formulated a series of policies and regulations to deal with the degradation of the ecological environment. For example, the Provisions on Land Reclamation was officially implemented on 1 January 1989; the Notice on the Strengthening of Land Reclamation Management for Production and Construction Projects was issued in 2006; and the Land Reclamation Regulations was issued by the State Council in 2011. From the implementation of the Provisions on Land Reclamation to the end of 2015, the ecological restoration rate of China's mining areas rose from 2% to 48% [63]. The results of ecological restoration in the mining area were also reflected in Yangquan Coal Mine. From 1987 to 2020, the ecological environment quality of Yangquan Coal Mine gradually changed to good and excellent. It is worth noting that in 2002, Yangquan City began to fully implement the project of returning farmland to forest and grassland, gradually returning slope farmland that is prone to soil erosion and wasteland suitable for afforestation into woodlands and grasslands. This has also been an important factor in the significant increase in the mean of the RSEI of Yangquan Coal Mine and its affiliated coal mines since 2002, which shows that the project of returning farmland to forest and grassland has significantly improved the ecological environment.

Before the 1990s, Yangquan coal mines mostly used the “top-down” natural dumping method to treat coal gangue, which could easily cause spontaneous combustion and landslides in the gangue dump. Since the 1990s, Yangquan Coal Mine has adopted a comprehensive technology of covering rolling and grouting for fire extinguishing to carry out the ecological restoration of coal gangue dumps. Due to failure to take measures such as vegetation restoration in time, the coal gangue dump after ecological restoration was destroyed by weathering and rain washing, resulting in repeated spontaneous combustion. In 2006, Yangquan Coal Mine formulated the ecological restoration mode of “slope cutting—leveling—rolling—fire extinguishing—soil covering—rolling—drainage system construction—vegetation planting—post maintenance”, and a large-scale ecological restoration project was carried out on the waste coal gangue dump. In 2011, Yangquan Coal Mine formulated the “top-down, layered discharge, loess covering, and restoration of vegetation” coal gangue discharge and disposal methods. As of the end of 2018, Yangquan Coal Mine had accumulated a total surface area of about 6.67 km² of coal gangue dumps, while all abandoned coal gangue dumps had completed ecological restoration. The continuous improvement of ecological restoration technology is an important factor in the rapid restoration of the ecological environment quality of coal gangue dumps.

In addition, Yangquan Coal Mine started to build large-scale photovoltaic power stations on the ground in the wasteland of the stable coal mining subsidence area, abandoned open-pit coal mines, and the relatively stable coal gangue dump in 2014, creating

a “photovoltaic + mine” characteristic ecological restoration method. Not only has the ecological environment been improved, but effective use of land has also been realized. Figure 6 shows that the ecological environment was improved after large-scale photovoltaic power stations were built on open-pit coal mines and coal mining subsidence areas, which is related to the characteristic ecological restoration method of “photovoltaic + mine”.

5.1.4. Urbanization Construction

In recent years, the impact and pressure of China’s urbanization on the ecological environment have become more and more obvious [64]. Urban expansion takes up a large amount of ecological land and production land, which reduces the surface vegetation coverage [65], increases the impervious surface area, and intensifies the urban heat island effect [28,55]. From 1987 to 2019, the area of construction land in the study area has doubled (Figure S1 and Table S2), the areas with fair and poor ecological environment have been moving closer to the central and northern urban areas year by year (Figure 6), and the spatial clustering characteristics are also low and low clusters (Figure 8). This shows that urbanization is one of the factors leading to the degradation of the ecological environment quality of Yangquan Coal Mine.

5.2. Limitations and Future Research Priorities

Using the RSEI after topographic correction to monitor and evaluate changes in the ecological environment of a coal mining area is a helpful means to discover the ecological environmental problems in the coal mining area and provide technical support for the development and planning of the coal mining area. However, due to the limited data, this study only analyzes the importance of topographic correction for ecological environmental quality assessment at the image level and lacks further verification of ground data. In addition, for sudden ecological environmental events outside the time range of remote sensing data, the RSEI can only observe the cumulative effects of the ecological environment, such as the sudden spontaneous combustion of coal gangue dumps and the rapid recovery of vegetation in coal mine areas in the short term, which will lead to the loss of part of the ecological environment inflection point information. Therefore, the focus of future research must be to improve the effectiveness of the RSEI in monitoring the ecological environment in coal mining areas. For example, multi-source remote sensing data fusion technology can be adopted to improve the temporal resolution of remote sensing data, and remote sensing data and ground data with key ecological attributes can be combined to assist the RSEI in carrying out ecological environment monitoring and evaluation.

6. Conclusions

This study introduced a topographic correction model to optimize the remote sensing ecological index (RSEI) and used the optimized remote sensing ecological index to comprehensively evaluate and analyze the temporal and spatial evolution of the ecological environment quality of Yangquan Coal Mine from 1987 to 2020. In addition, this article also described the driving forces behind the temporal and spatial evolution of ecological environment quality from two aspects: climate change and human factors. The result shows:

- (1) This study proved the feasibility of using topographic correction for ecological environmental quality assessment for the first time and provided new ideas for the improvement of ecological environmental quality assessment models. The NDVI is not sensitive to terrain, but topographic correction can further eliminate its terrain effects. Wet, the NDBSI, LST, and RSEI are sensitive to terrain and require topographic correction. The ecological environment quality evaluation model after topographic correction contains more information and is more representative than the ecological environment quality evaluation model without topographic correction. Therefore, we suggest that topographic correction should be used as a necessary element in data

- preprocessing in areas with large terrain fluctuations, which will help improve the practicability of the ecological environment quality evaluation model.
- (2) From 1987 to 2020, the mean of the RSEI of Yangquan Coal Mine and its affiliated coal mines showed an overall upward trend, while the proportion of good and excellent areas also continued to increase. The improved, unchanged, and degraded areas of the ecological environment of the entire study area accounted for 1339.23, 17.2, and 281.02 km², respectively. For the coal gangue dump, the ecological environment quality of D1, D2, D3, and D4 was generally improved, while the ecological environment quality of D5 and D6 was generally degraded.
- (3) The evolution of the ecological environment quality of Yangquan Coal Mine is the result of the combined effects of climate change and human factors, with human factors being the main driving force. Coal mining activities and urbanization have negative impacts on the ecological environment of Yangquan Coal Mine, while the increase in precipitation and the continuous development of ecological restoration have a positive impact on the ecological environment. Based on the results of stepwise regression analysis, greenness and dryness are the main indicators that determine the ecological environment quality of Yangquan Coal Mine, while humidity and heat are secondary indicators. Therefore, we suggest that the ecological restoration of coal mine areas in the future should focus on increasing vegetation coverage and reducing surface exposure. In coal gangue dumps with severe spontaneous combustion, it is also necessary to pay attention to fire prevention and cooling. For urban areas, the green construction of the city should be mainly ensured, while the speed of expansion and development direction of the built-up area should be reasonably controlled.

Supplementary Materials: The following are available online at <https://www.mdpi.com/article/10.3390/rs13142815/s1>, Table S1. Landsat remote sensing image used in this study; Table S2. Land cover area of the study area (km²); Table S3. Classification accuracy of land cover data; Table S4. Percentage change of ecological environment quality level within the boundaries of mineral rights from 1987 to 2020; Table S5. The mean value and standard deviation (SD) of each ecological environment index before and after SCS + C correction; Table S6. The contribution and load of the four variables to the first principal component (PC1) before and after SCS + C correction; Table S7. Pearson correlation coefficient between climate variables and the mean of RSEI. * Indicates that the correlation is significant at the 0.05 level; Figure S1. Land cover maps of the study area; Figure S2. Spatial distribution of RSEI grades of D1, D2 and D3 coal gangue dumps from 1987 to 2020; Figure S3. Spatial distribution of RSEI grades of D4 and D5 coal gangue dumps from 1987 to 2020; Figure S4. Land cover maps of the study area; Figure S5. Three-dimensional scatter plots of NDVI, Wet, NDBSI, LST and RSEI. (a) Three-dimensional scatter plots of NDVI, Wet and RSEI, (b) Three-dimensional scatter plots of NDBSI, LST and RSEI. The top of the scatter plot represents an area with better ecological environment quality, where the vegetation coverage is higher, the surface humidity is higher, the density of buildings and bare soil is lower, and the surface temperature is lower. The bottom of the scatter plot represents areas with worse ecological environment quality, where vegetation coverage is lower, surface humidity is lower, the density of buildings and bare soil is higher, and the surface temperature is higher; Figure S6. Scatter plots and fitted lines of ecological environment index values and cosi before and after SCS + C correction. (a) scatter plot and fitting line of NDVI and cosi before SCS + C correction, (b) scatter plot and fitting line of NDVI and cosi after SCS + C correction, (c) scatter plot and fitting line of Wet and cosi before SCS + C correction, (d) scatter plot and fitting line of Wet and cosi after SCS + C correction, (e) scatter plot and fitting line of NDBSI and cosi before SCS + C correction, (f) scatter plot and fitting line of NDBSI and cosi after SCS + C correction, (g) scatter plot and fitting line of LST and cosi before SCS + C correction, (h) scatter plot and fitting line of LST and cosi after SCS + C correction, (i) scatter plot and fitting line of RSEI and cosi before SCS + C correction, (j) scatter plot and fitting line of RSEI and cosi after SCS + C correction; Figure S7. The relative change rate of the mean value of each ecological environment index before and after topographic correction.

Author Contributions: Conceptualization, X.N. and Z.H.; methodology, X.N.; software, X.N.; validation, X.N., Z.H., and Q.Z.; formal analysis, X.N.; investigation, X.N., Z.H., Q.Z., and M.R.; resources, X.N.; data curation, X.N.; writing—original draft preparation, X.N.; writing—review and editing, Z.H.; visualization, X.N.; project administration, Z.H. and M.R.; funding acquisition, Z.H. All authors have read and agreed to the published version of the manuscript.

Funding: This research was funded by the National Key Research and Development Program (grant numbers: 2019YFC1805003 and 2020YFC1806505).

Institutional Review Board Statement: Not applicable.

Informed Consent Statement: Not applicable.

Data Availability Statement: The Landsat dataset is available from the United States Geological Survey website at <https://earthexplorer.usgs.gov/> (accessed on 13 May 2021). The DEM dataset is available from the Geospatial Data Cloud website at <http://www.gscloud.cn/> (accessed on 13 May 2021). The temperature and precipitation dataset is available from the China Meteorological Data Network at <http://data.cma.cn/> (accessed on 13 May 2021).

Acknowledgments: The authors thank anonymous reviewers for their constructive comments and suggestions which helped to improve the manuscript.

Conflicts of Interest: The authors declare no conflict of interest.

References

1. Zhou, A.; Hu, J.; Wang, K. Carbon emission assessment and control measures for coal mining in China. *Environ. Earth Sci.* **2020**, *79*, 1–15. [[CrossRef](#)]
2. Liu, S.; Li, W.; Qiao, W.; Wang, Q.; Hu, Y.; Wang, Z. Effect of natural conditions and mining activities on vegetation variations in arid and semiarid mining regions. *Ecol. Indic.* **2019**, *103*, 331–345. [[CrossRef](#)]
3. He, T.; Xiao, W.; Zhao, Y.; Deng, X.; Hu, Z. Identification of waterlogging in Eastern China induced by mining subsidence: A case study of Google Earth Engine time-series analysis applied to the Huainan coal field. *Remote Sens. Environ.* **2020**, *242*, 111742. [[CrossRef](#)]
4. Karan, S.K.; Ghosh, S.; Samadder, S.R. Identification of spatially distributed hotspots for soil loss and erosion potential in mining areas of Upper Damodar Basin—India. *Catena* **2019**, *182*, 104144. [[CrossRef](#)]
5. Ai, H.; Guan, M.; Feng, W.; Li, K. Influence of classified coal consumption on PM2.5 pollution: Analysis based on the panel cointegration and error-correction model. *Energy* **2021**, *215*, 119108. [[CrossRef](#)]
6. Luan, J.; Zhang, Y.; Tian, J.; Meresa, H.; Liu, D. Coal mining impacts on catchment runoff. *J. Hydrol.* **2020**, *589*, 125101. [[CrossRef](#)]
7. Fang, L.; Xinju, L.; Le, H.; Anran, S. A long-term study on the soil reconstruction process of reclaimed land by coal gangue filling. *Catena* **2020**, *195*, 104874. [[CrossRef](#)]
8. Zhou, N.; Yao, Y.; Song, W.; He, Z.; Meng, G.; Liu, Y. Present situation and prospect of coal gangue treatment technology. *J. Min. Saf. Eng.* **2020**, *37*, 136–146. [[CrossRef](#)]
9. Guo, W.; Chen, B.; Li, G.; Liu, M.; Liu, X.; Chen, Q.; Zhang, X.; Li, S.; Chen, S.; Feng, W.; et al. Ambient PM2.5 and Related Health Impacts of Spontaneous Combustion of Coal and Coal Gangue. *Environ. Sci. Technol.* **2021**, *55*, 5763–5771. [[CrossRef](#)]
10. Yang, Z.; Li, W.; Pei, Y.; Qiao, W.; Wu, Y. Classification of the type of eco-geological environment of a coal mine district: A case study of an ecologically fragile region in Western China. *J. Clean. Prod.* **2018**, *174*, 1513–1526. [[CrossRef](#)]
11. Zhao, W.; Yan, T.; Ding, X.; Peng, S.; Chen, H.; Fu, Y.; Zhou, Z. Response of ecological quality to the evolution of land use structure in Taiyuan during 2003 to 2018. *Alex. Eng. J.* **2021**, *60*, 1777–1785. [[CrossRef](#)]
12. Jing, Y.; Zhang, F.; He, Y.; Kung, H.; Johnson, V.C.; Arikena, M. Assessment of spatial and temporal variation of ecological environment quality in Ebinur Lake Wetland National Nature Reserve, Xinjiang, China. *Ecol. Indic.* **2020**, *110*, 105874. [[CrossRef](#)]
13. Song, W.; Song, W.; Gu, H.; Li, F. Progress in the remote sensing monitoring of the ecological environment in mining areas. *Int. J. Environ. Res. Public Health* **2020**, *17*, 1846. [[CrossRef](#)]
14. Rouse, J.W.; Haas, R.H.; Schell, J.A.; Deering, D.W. Monitoring vegetation systems in the Great Plains with ERTS. *NASA Spec. Publ.* **1974**, *351*, 309.
15. Yang, Z.; Li, J.; Zipper, C.E.; Shen, Y.; Miao, H.; Donovan, P.F. Identification of the disturbance and trajectory types in mining areas using multitemporal remote sensing images. *Sci. Total Environ.* **2018**, *644*, 916–927. [[CrossRef](#)] [[PubMed](#)]
16. Karan, S.K.; Samadder, S.R.; Maiti, S.K. Assessment of the capability of remote sensing and GIS techniques for monitoring reclamation success in coal mine degraded lands. *J. Environ. Manag.* **2016**, *182*, 272–283. [[CrossRef](#)]
17. Vorovencii, I. Changes detected in the extent of surface mining and reclamation using multitemporal Landsat imagery: A case study of Jiu Valley, Romania. *Environ. Monit. Assess.* **2021**, *193*, 1–24. [[CrossRef](#)] [[PubMed](#)]
18. Zhang, M.; Wang, J.; Li, S. Tempo-spatial changes and main anthropogenic influence factors of vegetation fractional coverage in a large-scale opencast coal mine area from 1992 to 2015. *J. Clean. Prod.* **2019**, *232*, 940–952. [[CrossRef](#)]

19. Song, Z.; Kuenzer, C.; Zhu, H.; Zhang, Z.; Jia, Y.; Sun, Y.; Zhang, J. Analysis of coal fire dynamics in the Wuda syncline impacted by fire-fighting activities based on in-situ observations and Landsat-8 remote sensing data. *Int. J. Coal Geol.* **2015**, *141–142*, 91–102. [[CrossRef](#)]
20. Syed, T.H.; Riyas, M.J.; Kuenzer, C. Remote sensing of coal fires in India: A review. *Earth Sci. Rev.* **2018**, *187*, 338–355. [[CrossRef](#)]
21. Yang, Y.; Zhang, Y.; Su, X.; Hou, H.; Zhang, S. The spatial distribution and expansion of subsided wetlands induced by underground coal mining in eastern China. *Environ. Earth Sci.* **2021**, *80*, 1–14. [[CrossRef](#)]
22. Yue, H.; Liu, Y.; Qian, J. Soil moisture assessment through the SSMMI and GSSIM algorithm based on SPOT, WorldView-2, and Sentinel-2 images in the Daliuta Coal Mining Area, China. *Environ. Monit. Assess.* **2020**, *192*, 237. [[CrossRef](#)]
23. Xu, J.; Yin, P.; Hu, W.; Fu, L.; Zhao, H. Assessing the ecological regime and spatial spillover effects of a reclaimed mining subsided lake: A case study of the Pan'an Lake wetland in Xuzhou. *PLoS ONE* **2020**, *15*, e238243. [[CrossRef](#)]
24. Xiao, W.; Lv, X.; Zhao, Y.; Sun, H.; Li, J. Ecological resilience assessment of an arid coal mining area using index of entropy and linear weighted analysis: A case study of Shendong Coalfield, China. *Ecol. Indic.* **2020**, *109*, 105843. [[CrossRef](#)]
25. Hou, H.; Ding, Z.; Zhang, S.; Guo, S.; Yang, Y.; Chen, Z.; Mi, J.; Wang, X. Spatial estimate of ecological and environmental damage in an underground coal mining area on the Loess Plateau: Implications for planning restoration interventions. *J. Clean. Prod.* **2021**, *287*, 125061. [[CrossRef](#)]
26. Firozjaei, M.K.; Sedighi, A.; Firozjaei, H.K.; Kiavarz, M.; Homae, M.; Arsanjani, J.J.; Makki, M.; Naimi, B.; Alavipanah, S.K. A historical and future impact assessment of mining activities on surface biophysical characteristics change: A remote sensing-based approach. *Ecol. Indic.* **2021**, *122*, 107264. [[CrossRef](#)]
27. Xu, H.; Wang, M.; Shi, T.; Guan, H.; Fang, C.; Lin, Z. Prediction of ecological effects of potential population and impervious surface increases using a remote sensing based ecological index (RSEI). *Ecol. Indic.* **2018**, *93*, 730–740. [[CrossRef](#)]
28. Xu, H.; Wang, Y.; Guan, H.; Shi, T.; Hu, X. Detecting ecological changes with a remote sensing based ecological index (RSEI) produced time series and change vector analysis. *Remote. Sens.* **2019**, *11*, 2345. [[CrossRef](#)]
29. Hu, X.; Xu, H. A new remote sensing index based on the pressure-state-response framework to assess regional ecological change. *Environ. Sci. Pollut. Res.* **2019**, *26*, 5381–5393. [[CrossRef](#)] [[PubMed](#)]
30. Shan, W.; Jin, X.; Ren, J.; Wang, Y.; Xu, Z.; Fan, Y.; Gu, Z.; Hong, C.; Lin, J.; Zhou, Y. Ecological environment quality assessment based on remote sensing data for land consolidation. *J. Clean. Prod.* **2019**, *239*, 118126. [[CrossRef](#)]
31. Firozjaei, M.K.; Fathololomi, S.; Kiavarz, M.; Arsanjani, J.J.; Homae, M.; Alavipanah, S.K. Modeling the impact of the COVID-19 lockdowns on urban surface ecological status: A case study of Milan and Wuhan cities. *J. Environ. Manag.* **2021**, *286*, 112236. [[CrossRef](#)] [[PubMed](#)]
32. Matsuoka, M.; Moriya, H.; Yoshioka, H. Correction of canopy shadow effects on reflectance in an evergreen Conifer Forest using a 3D point cloud. *Remote. Sens.* **2020**, *12*, 2178. [[CrossRef](#)]
33. Gao, M.; Gong, H.; Zhao, W.; Chen, B.; Chen, Z.; Shi, M. An improved topographic correction model based on Minnaert. *Gisci. Remote. Sens.* **2016**, *53*, 247–264. [[CrossRef](#)]
34. Riano, D.; Chuvieco, E.; Salas, J.; Aguado, I. Assessment of different topographic corrections in Landsat-TM data for mapping vegetation types. *IEEE T. Geosci. Remote* **2003**, *41*, 1056–1061. [[CrossRef](#)]
35. Teillet, P.M.; Guindon, B.; Goodenough, D.G. On the slope-aspect correction of multispectral scanner data. *Can. J. Remote Sens.* **1982**, *8*, 84–106. [[CrossRef](#)]
36. Civco, D.L. Topographic normalization of Landsat Thematic Mapper digital imagery. *Photogramm. Eng. Remote Sens.* **1989**, *55*, 1303–1309. [[CrossRef](#)]
37. Gu, D.; Gillespie, A. Topographic normalization of landsat TM images of forest based on subpixel sun-canopy-sensor geometry. *Remote Sens. Environ.* **1998**, *64*, 166–175. [[CrossRef](#)]
38. Yin, G.; Li, A.; Wu, S.; Fan, W.; Zeng, Y.; Yan, K.; Xu, B.; Li, J.; Liu, Q. PLC: A simple and semi-physical topographic correction method for vegetation canopies based on path length correction. *Remote Sens. Environ.* **2018**, *215*, 184–198. [[CrossRef](#)]
39. Gao, Y.; Zhang, W. A simple empirical topographic correction method for ETM + imagery. *Int. J. Remote Sens.* **2009**, *30*, 2259–2275. [[CrossRef](#)]
40. Soenen, S.A.; Peddle, D.R.; Coburn, C.A. SCS + C: A modified sun-canopy-sensor topographic correction in forested terrain. *IEEE T. Geosci. Remote* **2005**, *43*, 2148–2159. [[CrossRef](#)]
41. Vanonckelen, S.; Lhermitte, S.; van Rompaey, A. The effect of atmospheric and topographic correction methods on land cover classification accuracy. *Int. J. Appl. Earth Obs.* **2013**, *24*, 9–21. [[CrossRef](#)]
42. Dong, C.; Zhao, G.; Meng, Y.; Li, B.; Peng, B. The effect of topographic correction on forest tree species classification accuracy. *Remote Sens.* **2020**, *12*, 787. [[CrossRef](#)]
43. Huang, W.; Zhang, L.; Furumi, S.; Muramatsu, K.; Daigo, M.; Li, P. Topographic effects on estimating net primary productivity of green coniferous forest in complex terrain using Landsat data: A case study of Yoshino Mountain, Japan. *Int. J. Remote Sens.* **2010**, *31*, 2941–2957. [[CrossRef](#)]
44. Tian, X.; Li, Z.; Su, Z.; Chen, E.; van der Tol, C.; Li, X.; Guo, Y.; Li, L.; Ling, F. Estimating montane forest above-ground biomass in the upper reaches of the Heihe River Basin using Landsat-TM data. *Int. J. Remote Sens.* **2014**, *35*, 7339–7362. [[CrossRef](#)]
45. Jin, H.; Li, A.; Xu, W.; Xiao, Z.; Jiang, J.; Xue, H. Evaluation of topographic effects on multiscale leaf area index estimation using remotely sensed observations from multiple sensors. *Isprs J. Photogramm.* **2019**, *154*, 176–188. [[CrossRef](#)]

46. Zhu, Z.; Wang, S.; Woodcock, C.E. Improvement and expansion of the Fmask algorithm: Cloud, cloud shadow, and snow detection for Landsats 4–7, 8, and Sentinel 2 images. *Remote Sens. Environ.* **2015**, *159*, 269–277. [[CrossRef](#)]
47. Crist, E.P. A TM Tasseled Cap equivalent transformation for reflectance factor data. *Remote Sens. Environ.* **1985**, *17*, 301–306. [[CrossRef](#)]
48. Sobrino, J.A.; Jiménez-Muñoz, J.C.; Paolini, L. Land surface temperature retrieval from LANDSAT TM 5. *Remote Sens. Environ.* **2004**, *90*, 434–440. [[CrossRef](#)]
49. Roy, D.P.; Kovalskyy, V.; Zhang, H.K.; Vermote, E.F.; Yan, L.; Kumar, S.S.; Egorov, A. Characterization of Landsat-7 to Landsat-8 reflective wavelength and normalized difference vegetation index continuity. *Remote Sens. Environ.* **2016**, *185*, 57–70. [[CrossRef](#)]
50. Vidal-Macua, J.J.; Nicolau, J.M.; Vicente, E.; Moreno-de las Heras, M. Assessing vegetation recovery in reclaimed opencast mines of the Teruel coalfield (Spain) using Landsat time series and boosted regression trees. *Sci. Total Environ.* **2020**, *717*, 137250. [[CrossRef](#)]
51. Raynolds, M.K.; Walker, D.A. Increased wetness confounds Landsat-derived NDVI trends in the central Alaska North Slope region, 1985–2011. *Environ. Res. Lett.* **2016**, *11*, 85004. [[CrossRef](#)]
52. Xu, H. A new index for delineating built-up land features in satellite imagery. *Int. J. Remote Sens.* **2008**, *29*, 4269–4276. [[CrossRef](#)]
53. Rikimaru, A.; Roy, P.S.; Miyatake, S. Tropical forest cover density mapping. *Trop. Ecol.* **2002**, *43*, 39–47.
54. Seddon, A.W.R.; Macias-Fauria, M.; Long, P.R.; Benz, D.; Willis, K.J. Sensitivity of global terrestrial ecosystems to climate variability. *Nature* **2016**, *531*, 229–232. [[CrossRef](#)] [[PubMed](#)]
55. Hu, X.; Xu, H. A new remote sensing index for assessing the spatial heterogeneity in urban ecological quality: A case from Fuzhou City, China. *Ecol. Indic.* **2018**, *89*, 11–21. [[CrossRef](#)]
56. Guo, B.; Fang, Y.; Jin, X.; Zhou, Y. Monitoring the effects of land consolidation on the ecological environmental quality based on remote sensing: A case study of Chaohu Lake Basin, China. *Land Use Policy* **2020**, *95*, 104569. [[CrossRef](#)]
57. Martinez Batlle, J.R.; van der Hoek, Y. Clusters of high abundance of plants detected from local indicators of spatial association (LISA) in a semi-deciduous tropical forest. *PLoS ONE* **2018**, *13*, 93–115. [[CrossRef](#)]
58. Wei, W.; Guo, Z.; Xie, B.; Zhou, J.; Li, C. Spatiotemporal evolution of environment based on integrated remote sensing indexes in arid inland river basin in Northwest China. *Environ. Sci. Pollut. Res. Int.* **2019**, *26*, 13062–13084. [[CrossRef](#)] [[PubMed](#)]
59. Yan, X.; Li, J.; Shao, Y.; Hu, Z.; Yang, Z.; Yin, S.; Cui, L. Driving forces of grassland vegetation changes in Chen Barag Banner, Inner Mongolia. *GISci. Remote Sens.* **2020**, *57*, 753–769. [[CrossRef](#)]
60. Li, S.; Yang, B.; Wu, D. Community succession analysis of naturally colonized plants on coal gob piles in Shanxi Mining Areas, China. *Water Air Soil Pollut.* **2008**, *193*, 211–228. [[CrossRef](#)]
61. Li, S.; Liber, K. Influence of different revegetation choices on plant community and soil development nine years after initial planting on a reclaimed coal gob pile in the Shanxi mining area, China. *Sci. Total Environ.* **2018**, *618*, 1314–1323. [[CrossRef](#)]
62. Querol, X.; Izquierdo, M.; Monfort, E.; Alvarez, E.; Font, O.; Moreno, T.; Alastuey, A.; Zhuang, X.; Lu, W.; Wang, Y. Environmental characterization of burnt coal gangue banks at Yangquan, Shanxi Province, China. *Int. J. Coal Geol.* **2008**, *75*, 93–104. [[CrossRef](#)]
63. National Development and Reform Commission of China, National Energy Administration of China. *13th Five-Year Plan for Coal Industry Development*; National Development and Reform Commission (NDRC): Beijing, China, 2016.
64. Zheng, Z.; Wu, Z.; Chen, Y.; Yang, Z.; Marinello, F. Exploration of eco-environment and urbanization changes in coastal zones: A case study in China over the past 20 years. *Ecol. Indic.* **2020**, *119*, 106847. [[CrossRef](#)]
65. Yang, K.; Sun, W.; Luo, Y.; Zhao, L. Impact of urban expansion on vegetation: The case of China (2000–2018). *J. Environ. Manag.* **2021**, *291*, 112598. [[CrossRef](#)] [[PubMed](#)]